Heliyon 10 (2024) e38391

Contents lists available at ScienceDirect

Heliyon

journal homepage: www.cell.com/heliyon

Research article

QBD approach for green synthesis of Rutin silver nanoparticles-screening for antioxidant, anticancer and anticlastogenic potential

Harika Yadha [a], Rajini Kolure [b], Sneha Thakur [c,*], Kiranmai Mandava [d], Suhasini Boddu [b]

[a] Incozen Pharma, Hyderabad, India
[b] Department of Pharmacology, St. Pauls College of Pharmacy, Turkayamjal, Telangana, 501510, India
[c] Department of Pharmacognosy, St. Pauls College of Pharmacy, Turkayamjal, Telangana, 501510, India
[d] Department of Pharmaceutical Chemistry, St. Pauls College of Pharmacy, Turkayamjal, Telangana, 501510, India

ARTICLE INFO

Keywords:
Rutin
QbD
Silver nanoparticles
Drug release
Antioxidant
Anticancer

ABSTRACT

Rutin is a flavonoid glycoside abundant in many plants exhibiting pharmacological activities like antioxidant, anticancer, anti-inflammatory and antimicrobial activities. Plant biomarkers suffer low bioavailability and solubility that lack clinical effectiveness. The smart nanoparticles conversion addresses this limitation with optimal particle size and targeted drug delivery. The present study involves QbD approach for formulation of Rutin silver nanoparticles and evaluation of antioxidant, anticancer and anticlastogenic potential. QbD experimentation involved particle size and drug release as dependent variables over the silver nitrate concentration, methanol and sonication time as independent variables devising 15 formulations (F1 –F15). F12 formulation was found to be optimized with 126.3 nm average size, stable and dispersible characterized by UV, FTIR, SEM and DLS studies. The calibration curve of Rutin was plotted at 352 nm with linearity (LOD = 0.061 μg/ml and LOQ = 0.187 μg/ml). The *invitro* drug release studies by USP dissolution apparatus I (Basket type) proved the sustained release characteristics with 97.3 % drug release when compared to the Rutin. The pharmacological screening for potential antioxidant and anticancer activity on G361 and MCF 7 cell line of F12 formulation have shown promising results and also enhanced solubility in water compared to Rutin. Anticalstogenic potential as a function of induced micronuclei frequency was evaluated as a characteristic feature in bone marrow cells obtained from mice. Results indicate pre-treatment with the F12 reduced frequency of micronuclei in mouse bone marrow cells caused by Cyclophosphamide (CP) significantly. The protective effect of F12 in suppression was demonstrated at both dosages of 100 and 200 mg/kg. Thus the findings suggest the novel Rutin silver nanoparticles as lead drug serving as antioxidant, anticancer and anticlastogenic agent.

1. Introduction

Green chemistry is progressing science and the silver nanoparticles derived by this methodology are smart novel structures with reduced particles size, ecofriendly, and non toxic compared to chemical derived nanoparticles [1]. The green silver nanoparticles have

* Corresponding author.
E-mail address: snehathakur2189@gmail.com (S. Thakur).

https://doi.org/10.1016/j.heliyon.2024.e38391
Received 22 May 2024; Received in revised form 23 September 2024; Accepted 23 September 2024
Available online 24 September 2024

modified physicochemical and pharmacological properties enhancing their utility in drug modeling, 3-targeted drug delivery, diagnostics, and has commercial benefit [2]. Silver nanoparticles have marked therapeutic applications due to modified physcicochemical and biological properties commercially silver nanoparticles are trend in nanotherapeutics and diagnostics in treatment of diseases like cancer, rheumatoid arthritis, hepatitis, diabetes etc [3–7]. The progression of cancer is influenced by environmental, genetic, and nutritional factors. Mutagenic and carcinogenic agents, regardless of their origin, can cause DNA damage in humans [8,9]. In contrast to exogenous factors like physical and chemical carcinogens, endogenous factors also play a significant role in the transmission of biological effects. Endogenous contributing factors include hydroxyl and superoxide radicals as well as peroxide and oxygen radicals. A number of cancers, including as Hodgkin's disease, multiple myeloma, ovarian cancer, lung cancer, and breast cancer, have shown improvement in response to cyclophosphamide (CP) when combined with other medications that involves apoptotic cell signaling pathways and the cell modulation [10]. Adverse effects of CP treatment include bone marrow suppression, nephrotoxicity, increased infection risk, infertility, cardiovascular issues, and the development of secondary cancers [11,12]. The CP induced cytotoxicity are may be due to DNA arrays with inter/intra crosslinks, protein cross-links, and DNA monoadducts. DNA damage follows series of interrelated events, which include restoration of damage and apoptosis acceleration mechanisms. Cell death, genetic instability, and cancer can all be outcomes of CP's creation of micronuclei [13]. Exposure to CP increases the frequency of mutant red blood cells, which in turn damages cells for heamopoiesis and increases the risk of secondary leukemia. Research has proven CP with medication to be effective hence current future direction to target cancer cells more effectively while causing less harm to healthy cells. Genotoxicity screening involves micronucleus screening test and alkaline comet assay [14]. The formation of micronuclei (MN) occurs during cell division when a small acentric chromatin fragment is not fully segregated during anaphase. If a chromosome or chromosomal fragment is not totally separated during interphase, it becomes evident as a micronucleus. In order to facilitate rapid screening, the MN test was created as noted in Schmid method. Because of its ease of use, durability, sensitivity, and ability to detect DNA strand breaks reliably, the micronucleus test has become a popular screening method [15].

The toxicity of silver comparable to silver nanoparticles was found to be high with differed administration routes encountered various distribution patterns resulting in accumulation of silver in organs such as liver, kidneys, and lungs. Therefore, it is crucial to investigate the distribution patterns of green AgNPs compared to Ag + ions and to understand their toxicological effects [12,13]. The formulation of green silver nanoparticles must be carefully designed to modulate physicochemical parameters and minimize toxicity. QbD approach (box behnken design) with its module response surface methodology gives the best results for many independent variables of a design along with dependent variables to get the best performance [16–18].

The plant *Carica papaya* (Family-Papavaraceae) is a tropical Indian tree popular with antidengue, anticancer activity, also treating digestive problems and kills the intestinal worms [19–21]. The polar fractions of plant reveal phytochemicals like flavonoids, tannins, alkaloids, cardiac glycosides and also enzymes (Papain and chymotrypsin) [22]. Rutin, also known as vitamin P, is a low molecular weight flavonoid glycoside and polyphenol found widely in fruits, vegetables, and various herbs. It exhibits numerous pharmacological activities, including antiprotozoal, antibacterial, anti-inflammatory, antitumor, antiviral, antioxidant, hypocholesterolemic, anti-platelet, cardioprotective, and UV protective effects [23,24]. Rutin has poor bioavailability and limited water solubility; therefore, its modification into nanoparticles can enhance drug delivery by improving solubility and bioavailability, thereby overcoming these limitations [25,26]. Literature supports less data on the isolation of Rutin from leaves of *Carica papaya.* Further few studies have reported Rutin silver nanoparticles to be effective as anticancer agent and no support on its Anticalstogenic potential. There is limited literature on the sustained release characteristics and anticancer activity of Rutin silver nanoparticles, particularly in the context of skin and colon cancer.

Hence the study was oriented to synthesize and optimize the QbD Approach for formulation of Rutin silver nanoparticles and screen for *invitro* anticancer and antioxidant activities along with lime light on cancer mechanism with evaluation of *in vivo* anticlastogenic activity.

2. Materials and methods

2.1. Materials

The leaves of the plant *Carica papaya* were obtained from the local surroundings of Hyderabad, Telangana, India and were authenticated (voucher specimen KUW Acc.no-4986) by Dr. Ajmera Ragan, Professor, Department of Botany, Kakatiya University, Warangal, India.

2.2. Reagents and kits

All the reagents, chemicals and kits used for the study were of analytical grade and were procured from Sigma Aldrich chemicals, India.

2.3. Methods

2.3.1. Extraction, isolation and characterization of Rutin from Carica papaya leaves

The leaves of *Carica papaya* procured were thoroughly washed, cleaned and dried under shade for 7 days [18–22]. The dried leaves were coarsely powdered (1000 g) and loaded into the soxhlet apparatus then extracted with hexane, chloroform and methanol. Percentage yield was calculated using the formula.

$$Percentage\ yeild = \frac{Total\ weight\ of\ the\ dry\ extract}{Total\ weight\ of\ the\ plant\ material} * 100 \quad (I)$$

The methanol extract was subjected to column chromatography to yield Rutin in 30 % ethyl acetate and hexane fractions (Table 1). The isolated Rutin was characterized by UV-HPLC, NMR (H^1 and C^{13}) and MASS spectral methods (Figs. 1 and 2) (Table 3). TLC studies confirmed a yellowish brown spot in 30 % ethyl acetate in hexane. The isolated Rutin was further used to synthesize green silver nanoparticles and screen for *in vitro* anticancer and antioxidant activities [22,25,27].

2.3.2. Design of Experiment (DoE) for optimization of Rutin silver nanoparticles

For the product optimization of Rutin silver nanoparticles, QbD approach was adopted and software used for the quality product was Design expert software (version 13.0, Stat. Ease. Inc) with Box Behnken design (BBD) selected to get the product with less particle size [16–18]. The product profile could be optimized by taking silver nitrate concentration (Y1), solvent methanol (Y2) and sonication time (Y3) as independent variables reflecting the dependencies of product i.e Particle size, entrapment efficiency and cumulative drug release based on the literature (Table 3). The software was run to get the maximization of the process parameters and eliminate the minimal risk factors as shown in Table 2. The three factors were run at 3 levels (−1, 0, +1). The BBD design presents numerous advantages of optimization of product in shortest runs and understands the interaction effects of various factors in different levels. The studies were conducted in a random manner according to the program. According to the software's architecture, an optimum batch was created to calculate the relative error and deviation between the theoretical and practical approaches as seen in Table 6. Three-dimensional response surface plots were created to accurately ascertain the impact of factors [26–43].

2.3.3. Green synthesis of Rutin silver nanoparticles-concentration variation method

Various concentrations of Rutin dissolved in methanol were added to 0.1 M, 10 ml (1 mM) silver nitrate solution (4,7,10) and made up to 100 ml with distilled water. The mixture was kept for agitation at 400 rpm for 15 min and then at 200 rpm for overnight (Fig. 3A). The color change indicating reduction of silver ion by Rutin is observance of SPR peak shift to blue, as identified by UV–Vis spectrophotometry (UV3200, Lab India) (Fig. 3B). The formulation was obtained as cream amorphous powder characterized by DLS, SEM, XRD and FTIR analysis [24] determining particle size, shape and morphology [20].

2.4. Characterization of the rutin nanoformulation

Particle size and Zeta potential analysis by DLS: the Dynamic light scattering method (DLS) using Malvern Zetasizer (ZEN 3000) with process analytical control was used to determine the particle size and zeta potential of the nanoformulation. Experiment was conducted in triplicate at temperature of 25±2^o C and results are represented as Mean ± SD as in Tables 4 and 5.

Solid-state characterization: X- Ray diffraction method (XRD diffractometer, PAN) with Cu/ka radiation at 40 mA and 35 kV at 5–80 °C was operated to determine the crystalline nature and Differential scanning calorimetry (DSC, Shimadzu, 60 Calorimeter) studies were performed (see Table 6). Scanning electron microscope (SEM, JSM 50A Japan) was performed where the weighed amount of sample was placed on aluminium sealed pan heated at rate of 10 °C per minute from in dry nitrogen flow with rate of 20–40 mL/min with acceleration voltage of 15 kV.

2.4.1. Determination of entrapment efficiency

The standard calibration curve was plotted by UV–Vis studies at 352 nm as shown n Table 11. The entrapment efficiency of Rutin silver nanoparticles was measured using the ultra centrifugation technique. The overall volume of the preparation was examined, and 2 ml of the formulation was transferred to a centrifuge tube. The preparation was diluted with 5 ml of methanol and centrifugated at 2000 rpm for 20 min using a cooling centrifuge (Remi Instruments Ltd., India) in order to separate any undissolved matter. The liquid portion and solid portion were collected, and the volume of each was determined. The liquid portion was extracted and the untrapped medication quantity was determined using a UV–Visible spectrophotometer (UV3200, Lab India) at a wavelength of 352 nm (Table 2). The Rutin encapsulated in the nanoparticle formulation was determined by measuring the amount of Rutin entrapped and the amount that was subsequently extracted in the supernatant [28].

$$\%\ \text{Entrapment efficiency}\ \frac{\text{Total amount of drug} - \text{Amount of free drug}}{\text{Total amount of drug}} * 100 \quad (II)$$

2.4.2. Invitro drug release studies – dissolution studies

The therapeutic efficacy assessment with slow absorption is measuring the drug behavior on release *in vitro*. The *in vitro* drug release was evaluated using USP I basket type apparatus (Shimadzu, Japan) of SS16 grade immersed in water bath kept at neutral conditions at

Table 1
Physical status of *Carica papaya leaves* extracts.

S. no	Extract	Methanol extract	Chloroform extract	Hexane extract
1	Yield	118.6	85.9	58.6
2	Color	Reddish brown	Dark brown	Yellowish brown
3	Nature	Semisolid	Semisolid	semisolid

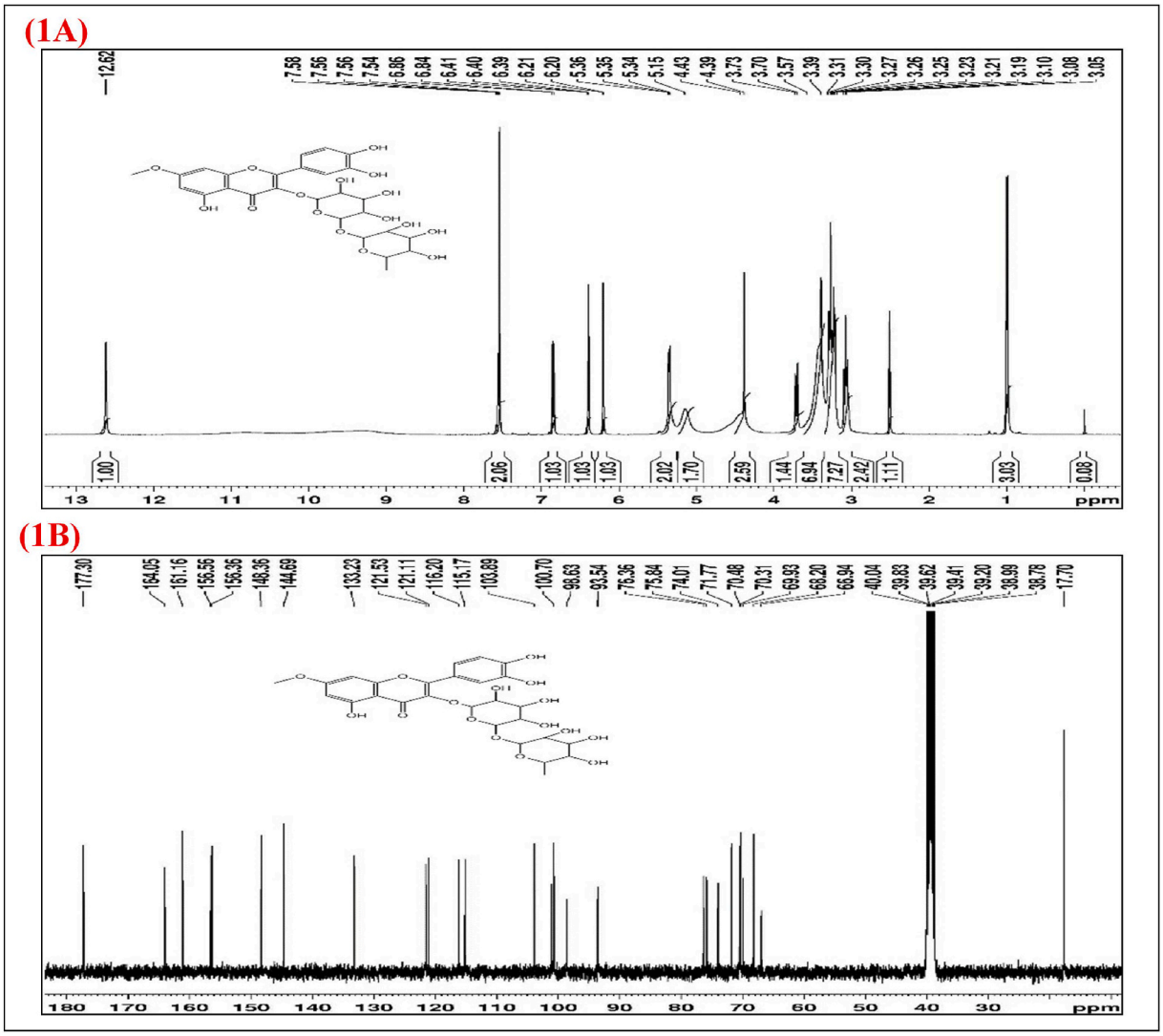

Fig. 1. (1A) H^1 NMR spectra of Rutin-3-O- Glycoside, (1B) C^{13} NMR of Rutin-3-O- Glycoside.

37 ± 2° C to determine the drug release as function of absorption from nanoparticles. The glass cylinder with 21# holds the test drug. The sample of weighed quantity is packed in cotton muslin cloth and kept inside the basket rotated at variable speed. The phosphate saline buffer (pH 7) was taken in the glass vessel (900 ml rotated at 100 rpm maintained in sink conditions. The withdrawn samples were analyzed by the UV–visible spectrophotometer at 352 nm for sample (Table 2). Based on the *invitro* results, the respective release kinetics (Table 13) were plotted of the cumulative percent release over the time profile [33–35].

Accelerated Stability studies: The optimized formulation was subjected to stability studies as per ICH Q1RA2 at 30–40 °C ± 2 °C and 65–75 % ± 5 % RH to determine the long term storage conditions. The formulation was place in USP Type I flint vial and sealed hermetically. They were stored further in humidity chambers (Thermofischer, India) for 90 days and evaluated or particle size and solubility after the storage period.

2.5. Invitro antioxidant activity

2.5.1. DPPH free radical scavenging assay

The conjugation between the phenoxide moieties of the molecules with the phenol moiety of the DPPH radical is a prominent effect of the reduction. 1.0 mg/ml of the F12 (Rutin silver nanoparticles), Rutin and the standard ascorbic acid were diluted serially to measured final concentrations of 5, 10, 25, 50, 125 and 250 μg/ml in methanol [27]. Then 2.6 ml of sample, test solution or Standard ascorbic acid were admixed with (0.3 mM) 1 ml of DPPH in methanol solution and left undisturbed for reacting at certain temperature for half an hour. The resulting reaction was carefully checked for Absorbance at 517 nm (Table 9) to predict the percentage inhibitory antioxidant activity (% AA) using the formula:

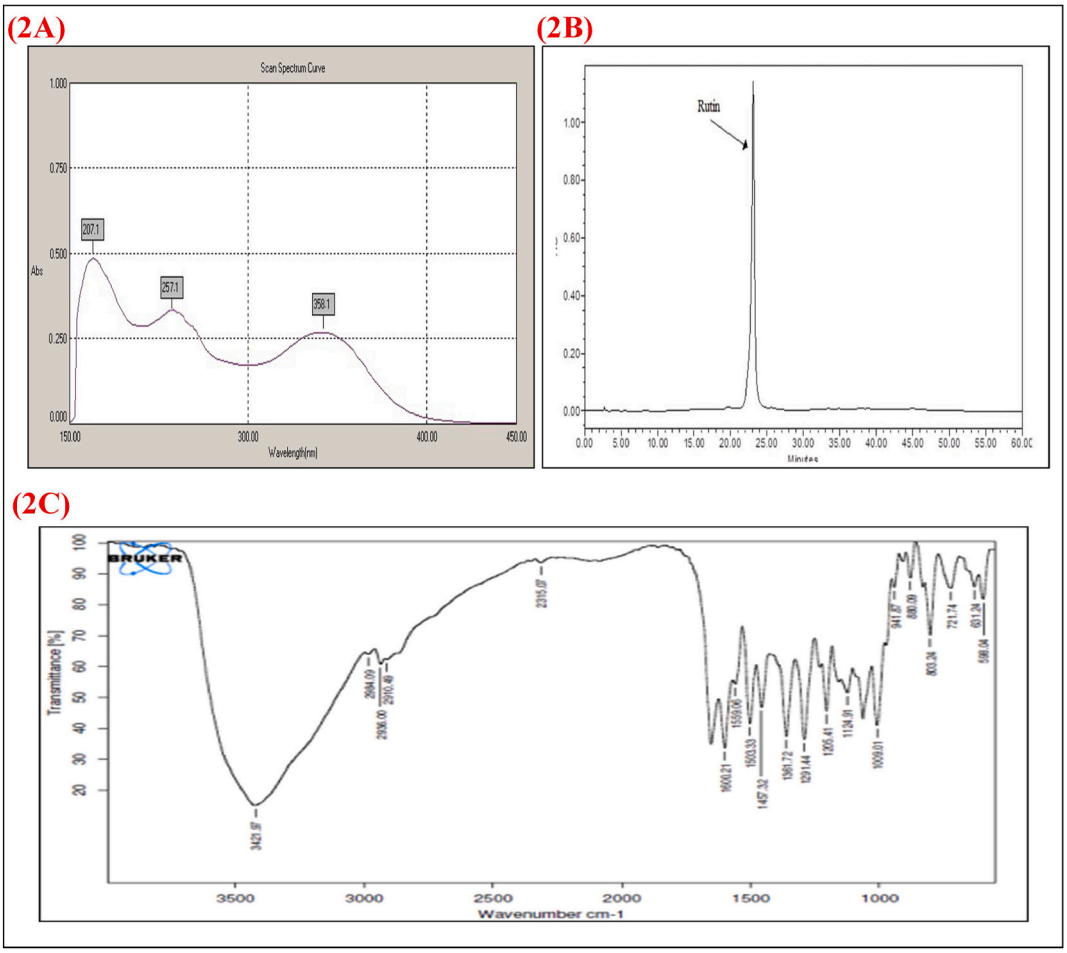

Fig. 2. (2A) UV Spectra of Rutin-3-O- Glycoside, (2B) HPLC of Rutin-3-O- Glycoside, (2C) FTIR spectra of Rutin-3-O- Glycoside.

Table 2
Formulation table for dependent and independent variables as per Box Behnken method (Variables and constraints used in Box-Behnken Design).

Std	Rutin	Factor X1$^{A:AgNO}$3 (ml)	FactorX2 B: solvent (ml)	FactorX3 C:Sonication time (min)	Response Y1 Particle size (nm)	Response Y2 Entrapment efficiency (%)	Response Y3 CDR %
1	1	4	20	5	89.2 ± 0.021	86.3 ± 0.23	86.1 ± 0.187
5	2	4	20	10	152 ± 0.01	76.5 ± 0.21	83.2 ± 0.1870.064
13	3	7	25	3.29552	123 ± 0.03	78.4 ± 0.25	85.1 ± 0.25
7	4	4	30	10	112 ± 0.1	82.2 ± 0.28	81.1 ± 0.123
12	5	7	33.409	7.5	147 ± 0.02	86.7 ± 0.21	92.6 ± 0.143
11	6	7	16.591	7.5	169 ± 0.01	75.4 ± 0.15	82.1 ± 0.031
15	7	7	25	7.5	154 ± 0.05	79.1 ± 0.18	83.5 ± 0.153
9	8	1.95462	25	7.5	132 ± 0.02	81.3 ± 0.24	91.7 ± 0.080
3	9	4	30	5	125 ± 0.015	76.6 ± 0.26	96.6 ± 0.053
2	10	10	20	5	148 ± 0.22	89.3 ± 0.12	93.6 ± 0.035
8	11	10	30	10	165 ± 0.26	85.5 ± 0.18	94.8 ± 0.665
6	12	10	20	10	126.34 ± 0.28	88.2 ± 0.023	97.3 ± 0.041
10	13	12.0454	25	7.5	187 ± 0.21	81.6 ± 0.56	92.4 ± 0.153
4	14	10	30	5	256 ± 0.45	82.1 ± 0.16	93.5 ± 0.023
14	15	7	25	11.7045	235 ± 0.23	83.1 ± 0.15	97.3 ± 0.056

$$\%\,AA = \frac{100 - [Abs - Abc]*100}{Abc} \quad \text{(III)}$$

Table 3
Process Variables in Box-Behnken design to optimize Rutin nanocrystals.

Variable	Name	Units	Low	Medium	High
X1	Silver nitrate solution	ml	4	7	10
X2	Methanol	ml	20	25	30
X3	Sonication time	min	5	7.5	10
Dependent variable		Factor	Units	Constraint	
Y1	Particle size	Y1	Nm	Minimize	
Y2	Entrapment efficiency	Y2	%	Maximize	
Y3	Cumulative drug release	Y3	%	Maximize	

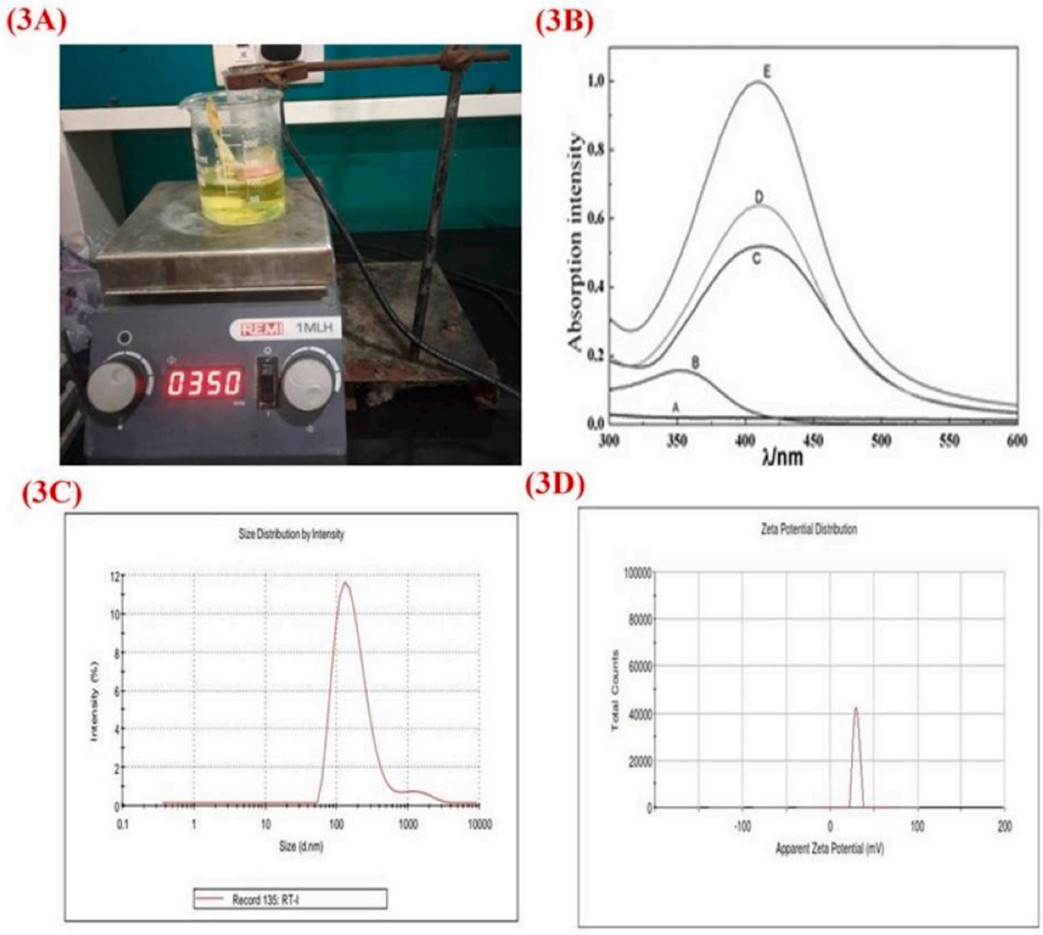

Fig. 3. (3A) Green synthesis of Rutin silver nanoparticles, (3B) SPR peak determination by UV Vis spectrophotometer, (3C) Particle Size of F12 by DLS, (3D) Zeta potential of F12 by DLS. (For interpretation of the references to color in this figure legend, the reader is referred to the Web version of this article.)

Where Abs = absorbance of sample and Abc = absorbance of control.

1 ml Methanol was taken as blank. 1 ml 0.3 mM DPPH with 2.6 ml Methanol was taken as negative control.

2.5.2. Reducing power assay

The reductive nature of test sample converts the ferri cyanide complex to the Fe^{2+} form and maintained by formation the Pearl's Prussian blue formation at 700 nm [28]. 1 mg/ml solution of standard and test samples were prepared and further the series of dilution (20,40,60, 80 and 100 μg/ml)solutions were admixed with 200 mM, 2.6 ml of pH 6.6 phosphate buffer and 30 mM, 2.6 ml of potassium ferricyanide. They were left undisturbed for 10–20 min at 60 °C. Then 2.6 ml of 600 mM trichloroacetic acid is admixed to reaction mixture and ultracentrifuge at 3500 rpm for 15 min. The supernatant layer 2.6 ml is separated along with 2.6 ml deionised water and

Table 4
C^{13} NMR δ values of Rutin.

C-position	δ C values
2	156.3
3	133.2
4	177.3
5	156.5
6	98.6
7	164.0
8	93.5
9	161.1
10	103.8
1`	121.5
2`	115.1
3`	144.6
4`	148.3
5`	116.2
6`	121.1
1''	100.7
2''	74.9
3''	76.3
4''	71.7
5''	75.7
6''	67.9
1'''	102.2
2'''	70.8
3'''	70.2
4'''	70.4
5'''	68.1
6'''	17.7 0

Table 5
Zeta potential of nanoformulations (F1-F15).

S. no	Mean (mV)
1	−22 ± 0.25
2	32 ± 0.01
3	23 ± 0.02
4	35 ± 0.01
5	47 ± 0.05
6	49 ± 0.01
7	34 ± 0.05
8	32 ± 0.21
9	25 ± 0.018
10	44 ± 0.20
11	35 ± 0.27
12	−28.6 ± 0.24
13	−27 ± 0.23
14	36 ± 0.42
15	−35 ± 0.13

Table 6
QbD response 1 of various process variables on particle size using Design Expert software Ver.12.

Source	Sum of Squares	Df	Mean Square	F-value	p-value	
Model	18348.09	9	2038.68	1.11	0.4794	Significant
A-Silver nitrate	7029.43	1	7029.43	3.83	0.1077	
B-Methanol	817.48	1	817.48	0.4455	0.5340	
C-Sonication time	1156.98	1	1156.98	0.6306	0.4631	
AB	2837.30	1	2837.30	1.55	0.2688	
AC	3307.28	1	3307.28	1.80	0.2371	
BC	2640.46	1	2640.46	1.44	0.2840	
A^2	63.57	1	63.57	0.0346	0.8597	
B^2	86.08	1	86.08	0.0469	0.8371	
C^2	80.80	1	80.80	0.0440	0.8421	
Residual	9173.86	5	1834.77			
Cor Total	27521.95	14				

Table 7
QbD response 2 Entrapment efficiency of various formulations using Design Expert software Ver 12 -ANOVA for Quadratic model.

Source	Sum of Squares	Df	Mean Square	F-value	p-value	
Model	122.20	9	13.58	0.6109	0.7549	significant
A-Silver nitrate	26.45	1	26.45	1.19	0.3251	
B-Methanol	7.48	1	7.48	0.3364	0.5871	
C-Sonication time	0.0739	1	0.0739	0.0033	0.9563	
AB	0.1012	1	0.1012	0.0046	0.9488	
AC	0.2813	1	0.2813	0.0127	0.9148	
BC	77.50	1	77.50	3.49	0.1208	
A^2	9.18	1	9.18	0.4130	0.5488	
B^2	7.19	1	7.19	0.3236	0.5941	
C^2	5.86	1	5.86	0.2637	0.6295	
Residual	111.12	5	22.22			
CorTotal	233.32	14				

Table 8
QbD response 3 Cumulative drug release of various formulations using Design Expert software Ver 12- ANOVA for Quadratic model.

Source	Sum of Squares	Df	Mean Square	F-value	p-value	
Model	309.52	9	34.39	0.9907	0.5350	significant
A-Silver nitrate	81.57	1	81.57	2.35	0.1859	
B-Methanol	40.30	1	40.30	1.16	0.3305	
C-Sonication time	3.71	1	3.71	0.1069	0.7570	
AB	15.12	1	15.12	0.4357	0.5384	
AC	68.45	1	68.45	1.97	0.2192	
BC	28.12	1	28.12	0.8102	0.4093	
A^2	56.96	1	56.96	1.64	0.2564	
B^2	11.96	1	11.96	0.3447	0.5827	
C^2	46.35	1	46.35	1.34	0.3001	
Residual	173.56	5	34.71			
CorTotal	483.08	14				

then 0.6 ml of 6 mM $FeCl_3$ is later added (Table 10). The reaction liquid is checked for absorbance at 700 nm. The standard ascorbic acid was used as a positive control.

2.6. In vitro anticancer activity on G361 and MCF7 cell line- MTT assay

2.6.1. Growth and Maintenance

G361 cells and MCF7 cells (ATCC) were sub cultured housed at Centre for Biiotechnology, JNTUH. The testing cells were grown in 75 cm^2 vented flask with DMEM and the grown cells appropriately were kept in neutral unreactive conditions like in a 6 % CO_2 at 37 °C humid containing conditions. Cells (passages 30–50) kept in Dulbecco eagles media (I.V gen, Paisley, UK) in filled with 10–12 % FBAS, 1–2% penicillin (1000U/ml), 1 % NE amino acids, 1 % amphitericin (250 U/ml)and 1 % streptomycin (1000 μg/ml). The cells were passaged enzymatically with EDTA 1 mM −0.25 % trypsin solution mixture and sub-cultured on 75 cm^2 plastic flasks at a density of 2.2-2.3x10^4 cells/cm^2. The replacement of culture medium was done each of two days. 80%Cell confluence was observed by microscopic study [28–30]. The treatment was performed 12 h post-growth to prevent cell differentiation. The volumes utilized for the protocol are for above flask .The culture medium was removed and discarded. The cell layer was rinsed briefly with combination of 0.53 mM EDTA -0.25 % (w/v) Trypsin solution to discard the traces of serum left that may have trypsin inhibitor. Then 2.-3 ml of Trypsin-EDTA liquid was portioned into the jar and the growth parameters of the cells were noted on an inverted advanced microscope till the layer of cells id suspended for 15min. Then 6–10 ml of total culture of grown cells with media were added with the aspiration of cells by pipette very slowly. Then the cell suspension aliquots were partitioned in to fresh culture containing jars. The cell lines were established in between 2 -4x 10^4 and 1-4 x 10^6 viable cells/cm^2. The upper limit not exceeding than the limit of 8x 10^8 cells/cm^2. The grown cell Cultures were maintained properly at 37 °C. The cell cultures were maintained at an interval of concentration between 8 x

Table 9
Effect of Ascorbic acid standard Rutin silver nanoparticles and Rutin on DPPH radicals.

Conc	log conc	Rutin silver nanoparticles	Rutin	STD
10	1	4.7 ± 0.03	1.7 ± 0.01	41.7 ± 0.03
20	1.30103	22.9 ± 0.04	19.4 ± 0.01	51.8 ± 0.02
30	1.4771213	35.4 ± 0.01	27.2 ± 0.02	81.9 ± 0.01
40	1.60206	42.8 ± 0.03	42.5 ± 0.04	89.4 ± 0.03
50	1.69897	51.5 ± 0.021	48.6 ± 0.03	94.6 ± 0.02
IC_{50}		49.7 ± 0.013	56.1 ± 0.015	30.6 ± 0.02

Table 10
Effect of Ascorbic acid standard, Rutin silver nanoparticles and Rutin by reducing power method.

Conc (μg/ml)	log conc	Rutin	Rutin silver nanoparticles	STD
20	1	0.41 ± 0.01	0.36 ± 0.01	0.49 ± 0.011
40	1.30103	0.49 ± 0.03	0.53 ± 0.022	0.56 ± 0.022
60	1.47712	058 ± 0.01	0.62 ± 0.013	0.68 ± 0.032
80	1.60206	0.69 ± 0.03	0.79 ± 0.015	0.89 ± 0.021
100	1.69897	0.86 ± 0.02	0.92 ± 0.018	0.956 ± 0.014

Table 11
Standard calibration curve of Rutin-Absorbance values.

S. no	Concentration μg/ml	Absorbance values				Standard deviation		
		Trial 1	Trial 2	Trial 3	Avg			
1	20	0.203	0.202	0.201	0.2018	0.001041	SE	0.05869
2	40	0.392	0.393	0.398	0.3933	0.004163	SD	0.17607
3	60	0.621	0.631	0.661	0.6376	0.020817	LOD	32.2795
4	80	0.781	0.812	0.813	0.802	0.018193	LOQ	97.8167
5	100	0.931	0.928	0.905	0.9213	0.014224		

Table 12
Cytotoxicity Of Rutin silver nanoparticles And Standard Doxorubicin On MCF 7 (Breast Cancer Cell Line) and G361 cell line (Human skin melanoma cell line).

		MCF 7 (Breast Cancer Cell Line)		G361 cell line (Human skin melanoma cell line)	
S. no	Concentration μg/ml	Rutin silver nanoparticles	Doxorubicin	Rutin silver nanoparticles	Doxorubicin
1	2.5	8.9 ± 0.010	20.8 ± 0.011	6.3 ± 0.011	25.3 ± 0.013
2	5	15.2 ± 0.021	55.3 ± 0.018	12.2 ± 0.026	56.2 ± 0.012
3	10	12.4 ± 0.011	62.8 ± 0.025	18.4 ± 0.015	72.5 ± 0.024
4	50	25.8 ± 0.03	72.3 ± 0.042	32.8 ± 0.034	83.2 ± 0.041
5	100	38.6 ± 0.024	79.6 ± 0.036	45.6 ± 0.022	89.6 ± 0.03
6	200	46.3 ± 0.032	86.5 ± 0.021	49.3 ± 0.035	93.1 ± 0.022
	IC_{50} value	29.65 ± 3.26	110.24 ± 2.65	118.36 ± 1.65	36.9 ± 2.45

Table 13
Kinetics of drug i.e drug behavior on release of Rutin silver nanoparticles (F12) and Rutin.

Drug kinetic model	F12	Rutin	Plot	Equation
Zero order	0.9504	0.8551	Q_t vs t	$Q_t = K_0\ t$
First order	0.9836	0.9774	$In(Q_o - Q_t)$ vs t	$In\ Q_t = In\ Q_o - K_1 t$
Higuchi	0.9831	0.9432	Q_t vs $t_{1/2}$	$Q_t = K_h t^{1/2}$
Korsmeyer peppas	0.9771	0.9564	Q_t vs log t	$\ln(Qt) = \ln(kKP) + n\ln(t)$

10^4 -10^6 cell/cm^2. Sub cultivation Ratio was followed at 1:2–1:4 ratio with periodical renewal of medium for about 2–5 cycles per week [29,31].

3. Assay procedure

G361 and MCF 7 cells (100 μl per tube well) were plated and sub cultured in a 98-cell depth well clear bottom culturing plates (10^6 cells/well). F12(Rutin silver nanoparticles) with concentration of 100 and 250 μg/ml are added after a day seeding and well maintained in conditions for about 3 days. 2 μL volumes of growth media is utilized two times for the all samples. The culture is removed and the washed twice using PBS. 16 μL of methyl tetrazolium indicator per culture well is admixed and volume is noted in PBS medium to 0.6 mg/ml final concentration. The reagent volume is continuously supervised based on the volume of growth culture and the grown cells are monitored by keeping them for 3–4 h at room temperature till the indicator color changes to purplish shade visible under microscope [27–29] Methyl tetrazolium indicator was removed and added with 10 μL DMSO to each well with slow stirring at constant temperature. The Absorbance is measured at 570 nm for each well using axiovert plate reader. G361 and MCF7 Cells was tested after seeding post 12h with 100 μg/ml, 250 μg/ml concentration of sample for morphological study. Cells were observed for each day after treatment of sample samples [31]. The cell viability was calculated according to the formula. The anti-proliferative potential of the extracts was tested via MTT assay on MCF7 cell line against the standard Doxorubicin. The IC_{50} values were determined and tabulated

(Table 12, Fig. 10). The histogram for cell survivability was constructed by using Graph Pad Prism Software 5.0.

$$\text{Cell survivability (\%)} = \frac{\text{mean OD of treated cell} - \text{mean OD of blank} \times 100\%}{\text{mean OD of untreated cell} - \text{mean OD of blank}} \quad \text{(IV)}$$

4. Animals used in experiments

The study was carried out on Swiss albino mice that were kept at the animal facility of St. Pauls College of Pharmacy in Telangana, India. The mice were kept in a temperature-controlled room for 24 h at a constant temperature of 27 ± 2 °C, with a relative humidity of 40–50 %. They were housed in cages that were similar to polypropylene shoe boxes and were provided with pellets from Amruth Feeds, India, as well as free access to water. The experiments were performed on rats that were 8–10 weeks old and had an average weight of 25 ± 2 g.

4.1. In vivo toxicity studies

4.1.1. Acute oral toxicity studies

The animals were carefully chosen and then separated into three groups, with each group consisting of three animals. The control group received distilled water (2 mL/kg) while the experimental group received SNPs. Graded doses of the F12 (100, 200, 300, 600, 800, 1000, and 2000 mg/kg) were given to the other groups as per OECD guideline for Acute toxic class method 423 [41]. Following the administration, the animals were consistently monitored for any alterations in behavior or mortality within the initial 4-h period. Subsequently, they were intermittently observed for the following 6 h, and then once more at the 24-h mark after dosing. Subsequently, they were monitored for a maximum of 14 days post administration to determine if there were any deaths.

4.1.2. Bone marrow micronucleus test

4.1.2.1. Administration and regimen. The study consisted of six distinct groups: a control group, two groups treated with F12, a group treated with CP, and two groups receiving a combination of F12 and CP at different doses. Thirty-six Swiss albino mice were randomly divided into six groups. Each group was provided with a total of six animals, consisting of three males and three females, who were kept in individual enclosures [28,39,40]. The animal care and experimentation adhered to protocols that were approved by the CCSEA. By following the prescribed protocols and upholding the utmost moral principles, we provide optimal care for each variety of animals. Before doing any animal testing, the Institutional Animal Ethics Committee (IAEC) of St. Pauls College of Pharmacy in Turkayamjal, Telangana, India, thoroughly examined and granted approval for all experimental procedures (IAEC/SPCP/PCOG01/2022) [37].

Our investigation contained two distinct dosages of F12 (0.1 and 0.2 g/kg, b.w) based on acute oral toxicity results. The control group was administered normal saline orally. The positive control group received a single dose of cyclophosphamide (CP) at a dose of 0.04 g/kg/bw intraperitoneally. The treatment group was pre-treated with F12 orally at doses of 0.1 and 0.2 g/kg/bw for 14 days, and cyclophosphamide was administered 1 h before the last dose of F12. The bone marrow cells of mice were dissected and altered for the purpose of conducting a micronuclei assay. This was done after subjecting the cells to a treatment for duration of 24 h.

5. Procedure

The bone marrow micronucleus (BMN) assay was conducted using the Schmid method, with some adjustments as described by Seetharam et al. in compliance with the OECD recommendation (474). After adding 2 mL of a solution containing three percent bovine serum albumin (BSA) to the bone marrow cells extracted from the tibia and femur bones, the resulting mixture was centrifuged at a speed of 1500 rpm for duration of 10 min. After removing the supernatant, the pellet was re-suspended in the required amount of 3 % BSA to provide the correct thickness solution. A suspension drop was administered onto a clean slide, left to dry naturally, and subsequently immersed in methanol for duration of 10 min. The fixed slides were treated with Giemsa stain for 10 min and May-Grunwald's stain for 15 min. Following a double or triple rinse in phosphate buffer, the slides were immersed in distilled water for 1 min to facilitate the appropriate distinction between immature and adult erythrocytes. Using an Olympus BX51 microscope, the slides were examined to confirm the presence of micronuclei in poly and normochromatic erythrocytes (PCE and NCE). NCE staining is reddish pink, whereas PCE staining is blue. Additionally, the PCE/NCE ratio was calculated using this data. A total of 2000 PCE and matching NCE observed in the field were examined for the presence of MN in each animal (Table 14).

6. Statistical analysis

Data were expressed as mean values of three experiments ($n = 3$) ± SD. Correlation between analysis of antioxidant activity and the anticancer activity were carried out using the correlation and regression applications in the Microsoft Excel version windows 10. The i*nvitro* Cytotoxicity activity was evaluated by Statistical analysis between treated cells and untreated cells was done using one way ANOVA followed by Dunnett's multiple comparison test. *$p < 0.05$, and ***$p < 0.001$ denoted significant difference as compared to untreated cells (control). One way ANOVA and Dunnett's test post hoc performed in Graph Pad Prism 9 determined the statistical significance (Graph Pad Software, Inc., CA, USA). Comparisons reflected between the RSNP treatment groups and a control group. Groups receiving CP treatment were compared to those receiving RSNP + CP. P-value ≤0.05 indicate statistical significance or

indifferences. Results were considered significant if they were labelled as $^{*\#}P < 0.01$, and $^{**\#\#}P < 0.001$.

7. Results and discussion

7.1. Extraction, isolation of rutin-3-O glycoside from methanolic extract of Carica papaya leaves

The percentage yield of the methanol extract was found to be 118.6 %, reddish brown in color and semi solid in nature. The chloroform extract was obtained in 85.9 % yield, dark brown in color and semisolid in nature. The hexane extract was obtained in 58.6 % yield, yellowish green in color and sticky semi solid in nature (Table 1). The qualitative analysis of the methanol, chloroform and hexane extracts of *Carica papaya* as revealed polar constituents such as alkaloids, glycosides, flavanoids, steroids and terpenoids. The methanol extract was subjected to column chromatography to isolate the Rutin. The methanolic extract was subjected to column chromatography which could yield Rutin in 30–50 percent ethyl acetate in hexane fractions and later identified using UV-HPLC, NMR and MASS spectrometric techniques.

8. Characterisation of Rutin

1. H^1 and C^{13} NMR analysis

The structure of Rutin (was confirmed by $H^1$and C^{13} NMR studies. The H^1, C^{13} NMR (Fig. 1A and B) could reveal the nature of hydrogens and carbons at different positions which could estimate the flavanoids moiety of the Rutin. In the ^{13}C NMR spectrum, the terminal sugar was determined as a rhamnose by low field chemical shift of glucose C-6 methylene (67.9). The carbon signals at δ 100.7 and δ 102. 2 showed glucosyl C-1″ and rhamnosyl C-1‴ respectively Table 4)

2. UV- HPLC and FTIR analysis

The UV- HPLC (Fig. 2A and B) was carried out on Shimadzu. The RP- HPLC analysis was performed using a Water modular system consisting of two model 1525 pumps, an automatic gradient controller, a model 717 plus injector, a model 2996 Photodiode array detector (PAD) and empower software. The injector, gradient controller and chromatography manager were integrated together to Fig. 4) give reproducible results. Phenomenex Sphereclone ODS2 column (4.6 × 250 mm, 5 μm) was used for the analysis, and spectral acquisition was performed at 352 nm after scanning the maximum plot of standard.The FTIR studies were done on Bruker FTIR using KBR pellet method. FTIR analysis revealed sharp peaks at 3429, 2930, 2910, 2890, and 2876 cm^{-1}, indicating the C-3 alcohol of catechol. Peaks at 1457 and 1389 cm^{-1} suggest the presence of C=C alkene groups. The peaks at 1078-830 indicate the alkyl groups (Fig. 5).

8.1. Experimental design and optimization

The nanocrystals of Rutin were synthesized using the QbD approach in which quality process attributes were identified. Design of Experiment (DoE) was applied to process parameters to reach the optimization. A total of 24 runs were performed using BBD to report the responses as in Table 2. The observed responses were analyzed using Design-Expert software (Trial version 10; Stat-Ease Inc., USA) and fitted into different models, such as linear and quadratic, to evaluate the impact of the components. The independent variables were discovered and their impact on the dependent variables was examined using one-way ANOVA and three-dimensional (3D) graphs. The plots facilitate the examination of the impact of factors on the replies and assist in evaluating the simultaneous interaction effect of three elements. The subsequent section examines the model produced for each of the dependent variables and their impact on the answers. The BBD was found to be marginally more efficient than other response surface designs, although it has shown significantly greater efficiency than the 3-level complete factorial design. Silver nitrate is essential in the creation of nanocrystals as a complexing agent. Methanol was employed as a solvent to improve solubility and facilitate precipitation. The duration of sonication inhibits additional particle agglomeration.

Table 14
Frequency of MN in Cyclophosphamide- and F12-treated mice's bone marrow cells.

Treatment (mg/kg)	MNPCE (%)	Total MN (%)	PCE/NCE
Control (0.9 % saline)	0.0.15 ± 0.09	0.08 ± 0.012	1.56 ± 0.036
Positive control (CP-40)	4.12 ± 0.135**	2.84 ± 0.052**	0.89 ± 0.017**
F12-100	0.13 ± 0.07##	0.06 ± 0.024##	1.74 ± 0.012##
F12-200	0.10 ± 0.013##	0.05 ± 0.011##	1.58 ± 0.006##
F12-100 + CP-40	2.57 ± 0.041##	0.74 ± 0.013##	0.85 ± 0.037##
F12-200 + CP-40	1.54 ± 0.004##	0.56 ± 0.011##	0.62 ± 0.014##

Mean ± Standard error of the mean (n = 6) is how the values are shown. 2000 PCE scored for every animal. Analysis of variance (ANOVA) with a post hoc Dunnett's test. Significant at the $^{**}P < 0.001$ level when compared to the control group. $^{\#\#}P < 0.001$ when compared to cyclophosphamide.

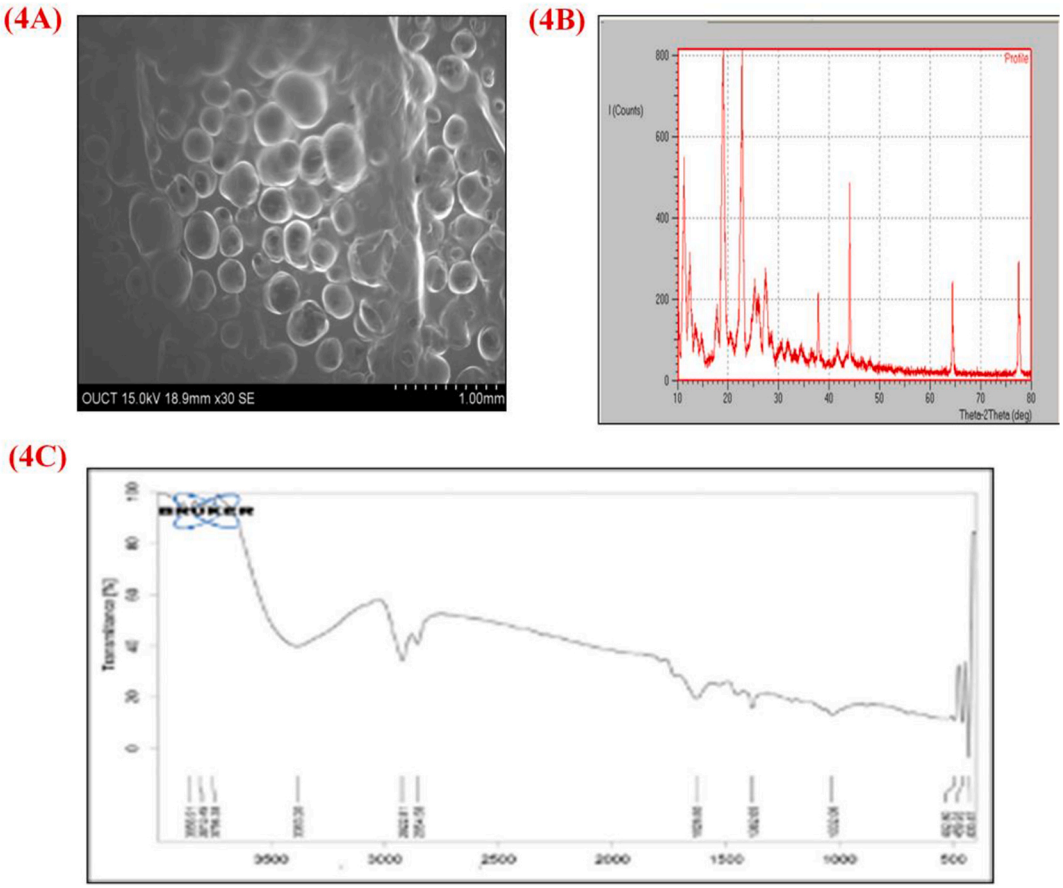

Fig. 4. (4A) SEM micrograph determining spherical morphology, (4B) XRD micrograph determining crystalline nature, (4C) FTIR graph of F12 determining no agglomeration.

8.2. Effect of independent variables on particle size

The solubility of nanocrystals and the bioavailability of drug rely on determined by the particle size. The average particle size of Rutin nanoparticles was 554.68 nm, whereas the size of nanocrystals ranged from 89.2 ± 0.021 to 256 ± 0.45 nm. BBD proposed a linear model to describe the impact of particle size. The correlation between the coded components and particle size was evaluated using Equation V and 3D graphs. The results are tabulated in Table 2 and the influence of the dependent variables in form of response surface graphs was reported in Fig. 7A, B and 7C. The linear polymeric equation is shown in equation V reflecting the effect of various dependet variables on the particle size.

$$\text{Particle size} = 540.57 - 47.64A + 91.22B - 139.43C \quad \text{(V)}$$

As per the ANOVA optimization results, a F-value model of 1.11 was obtained suggesting a significance in linear model. There is only 0.47 % probability that F-value is large could be due to noise with model parameters to be significant. As per the equation, the silver nitrate concentration(A) and sonication time(C) had a marked effect on the particle size (P, 0.05). The silver nitrate concentration is increased and there by the reducing activity of Rutin enhances thus the particle size varies based on the varying sonication speed at neutral temperature 25± 2 °C. This can be attributed to the polyphenolic nature of Rutin that helps in reduction and neutralization of silver nitrate. There was minimal solvent effect of methanol as per the analysis by QdD approach.

8.3. Effect of independent variables on entrapment efficiency

The quadratic model was followed as per BBD design which showed significant impact of process parameter on entrapment efficiency which determines key motive in loading capacity of drug. The results demonstrated in Table 7 and effect in form of response surface methodology was shown in Fig. 8A, B and 8C that the drug entrapment efficiency significantly improved from 58.56 ± 6.94 to 89.3 ± 0.12 when the silver nitrate: drug ratio in the formulation (Table 7). Notably, formulation E3 exhibited the highest entrapment efficiency, with statistical significance ($P < 0.05$).

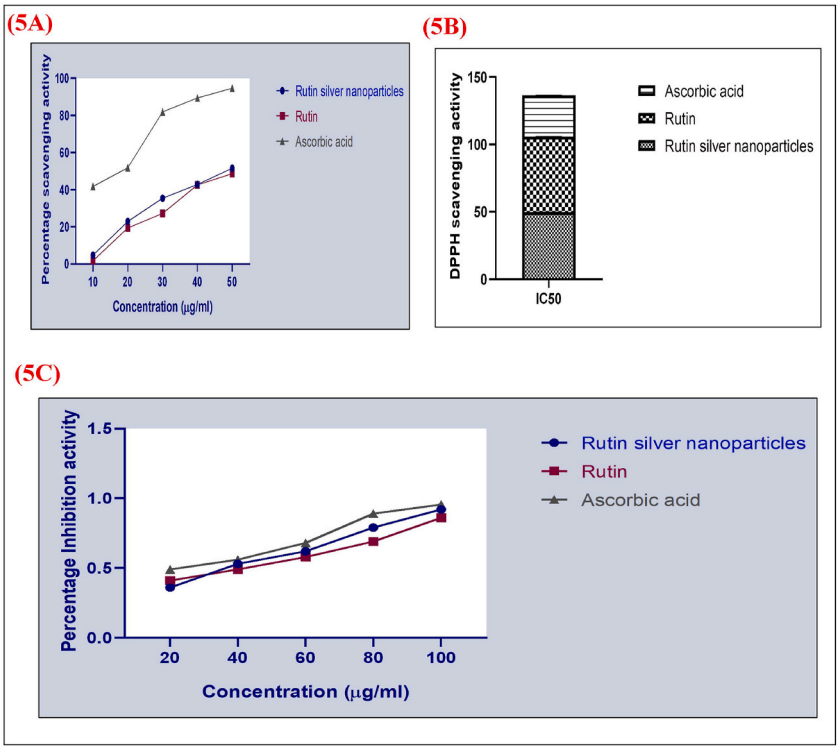

Fig. 5. (5A) Percentage inhibitions of Rutin silver nanoparticles and Rutin over standard ascorbic acid by DPPH assay, (5B) IC_{50} Value determination by DPPH assay, (5C) Reducing capability of Rutin silver nanoparticles and Rutin over standard Ascorbic acid by reducing power assay.

8.4. Effect of independent variable on cumulative drug release

The nanoparticle formulations, with silver nitrate to drug ratios of 4:1, 7:1, and 10:1, exhibited an increase in drug release ranging from 81.1 ± 0.123 % to 97.3 ± 0.056 % over a period of 24 h as shown in Table 8. This was in contrast to the sustained release nature of Rutin, which was utilized as the control. The release patterns of nanoparticle formulations indicate an initial rapid release, possibly caused by the drug being adsorbed onto the surface of the nanoparticles, followed by a sustained release due to the drug being encapsulated within the nanoparticles. The one-way analysis of variance (ANOVA) and Box-Behnken design (BBD) optimization have demonstrated that the concentration of silver nitrate and sonication period have a significant influence on the design of cumulative drug release ($P < 0.05$) as shown in Fig. 9A, B and 9C.

8.5. Green synthesis of silver nanoparticles of rutin

The isolated Rutin-3-O-glycoside was utilized as reducing agent and internal capping agent to synthesize the silver nanoparticles. The Rutin 0.1 mM solution (10 mg in 1 ml methanol) was dissolved and 10 ml of 0.1 M, 0.3M and 0.5 M silver nitrate solution was added, kept for agitation at 900 rpm at 37 °C over night on a magnetic stirrer and observed for colour change (Fig. 3A). The pale yellow colored Rutin solution changed to dark brown indicating the formation of silver nanoparticles as observed to be SPR peak in UV–Vis spectrophotometer and also the size, shape and morphology was confirmed by DLS, SEM and XRD studies.

9. Characterization of Rutin silver nanoparticles

9.1. Particle morphology-DLS, FTIR and UV–vis studies

The DLS studies were carried out by Malvern Zeta sizer which revealed the size of Rutin silver nanoparticles was found to be 126 nm (Fig. 6) by average 90 % of the particles and the zeta potential value was found to be −28.6 mV by 90 % of the particles which confirms that the Rutin silver nanoparticles were stable as the zeta potential value was found to be ≤ 30 mV(Fig. 3A and D). The SPR peak was blue shifted from 352 nm (Fig. 3B) to 426 nm which indicates the characteristic formation of silver nanoparticles. The increase in the wavelength indicates the stabilization of silver and also the reduction of silver ion by Rutin, acting as internal stabilizing and capping agent for silver ion. The FTIR analysis (Fig. 4C) could reveal that the Rutin acts as stabilizing and internalizing capping agent for the reduction of silver ions. The peaks at 600-700 cm^{-1} indicates the reduction of silver ion. The peaks at 3400-2900 cm^{-1} indicate the functional group region of the Rutin-3-O-glycoside. Further there was no agglomeration observed.

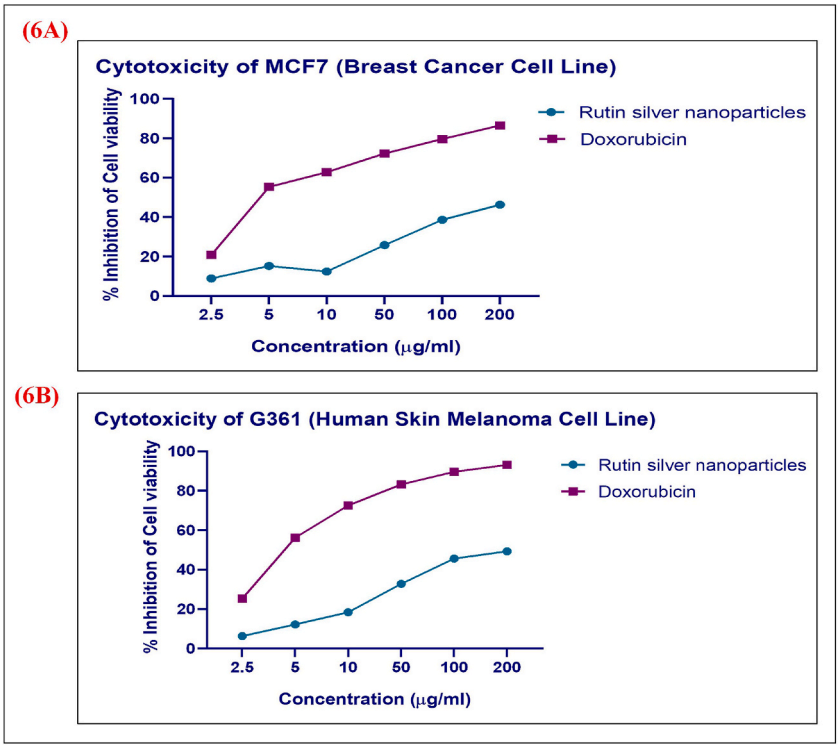

Fig. 6. IC_{50} value determination by MTT assay for the optimized F12 formulation in G361 and MCF 7 cell lines. Different cell grouped (G361-skin cancer and MCF7 – breast cancer) were treated with standard Doxorubicin and F12 (Rutin silver nanoparticles) formulation at various concentrations(from 2.5 to 100 µg/ml) and the cell viability was measured with MTT assay. (6A) Results of MTT detection in G361 cell line, (6B) Results of MTT assay detection in MCF7 cell line.

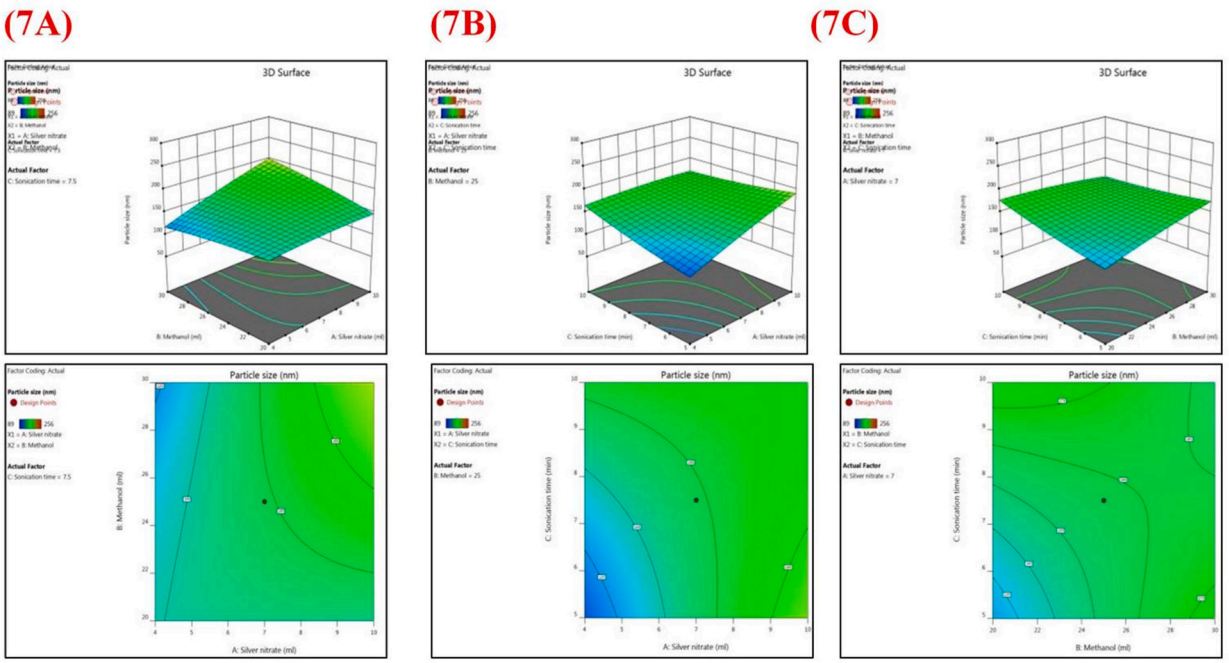

Fig. 7. 3D responsive plots – showing the effect of independent variables on particle size Three-dimensional plots showing the effect of independent variables on particle size. Notes: (7A) Effect of solvent and silver nitrate on particle size, (7B) Effect of sonication time and silver nitrate concentration on particle size, (7C) Effect of sonication time and methanol on particle size.

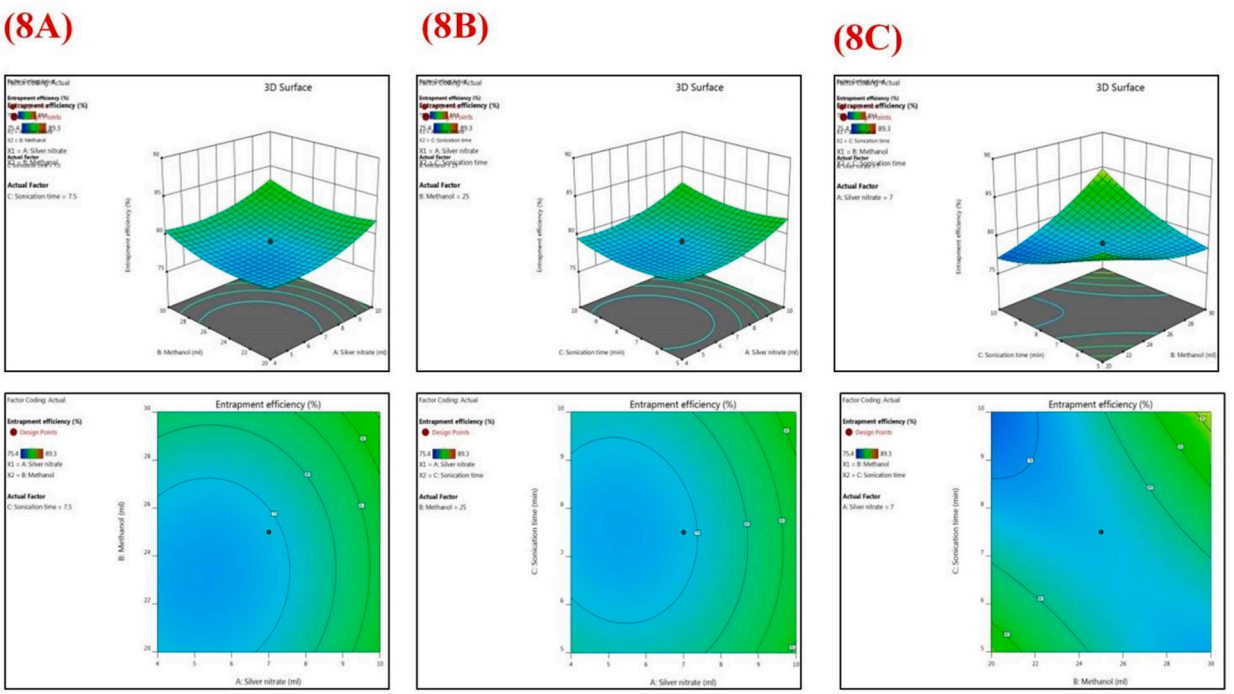

Fig. 8. 3D responsive plots – showing the effect of independent variables on entrapment efficiency: Three-dimensional plots showing the effect of independent variables on entrapment efficiency. Notes: (8A) Effect of solvent and silver nitrate, (8B) Effect of sonication time and silver nitrate concentration, (8C) Effect of sonication time and methanol.

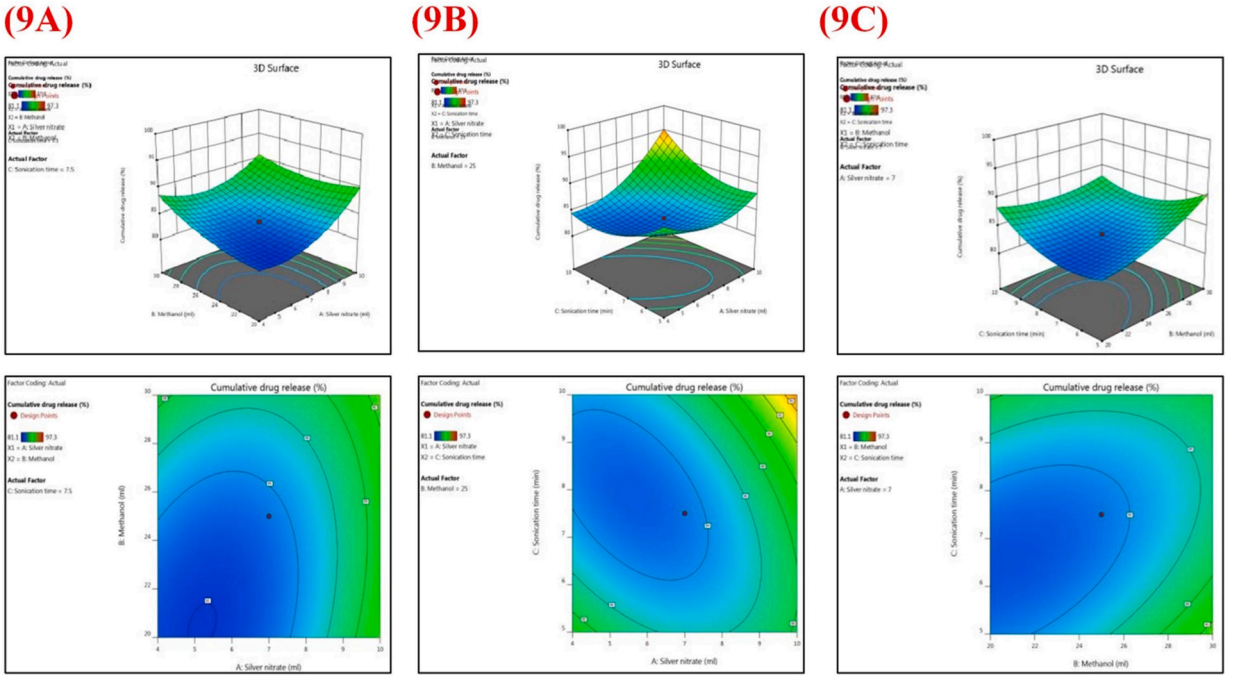

Fig. 9. 3D responsive plots – showing the effect of independent variables on Cumulative drug release: Three-dimensional plots showing the effect of independent variables on Cumulative drug release. Notes: (9A) Effect of solvent and silver nitrate, (9B) Effect of sonication time and silver nitrate concentration, (9C) Effect of sonication time and methanol.

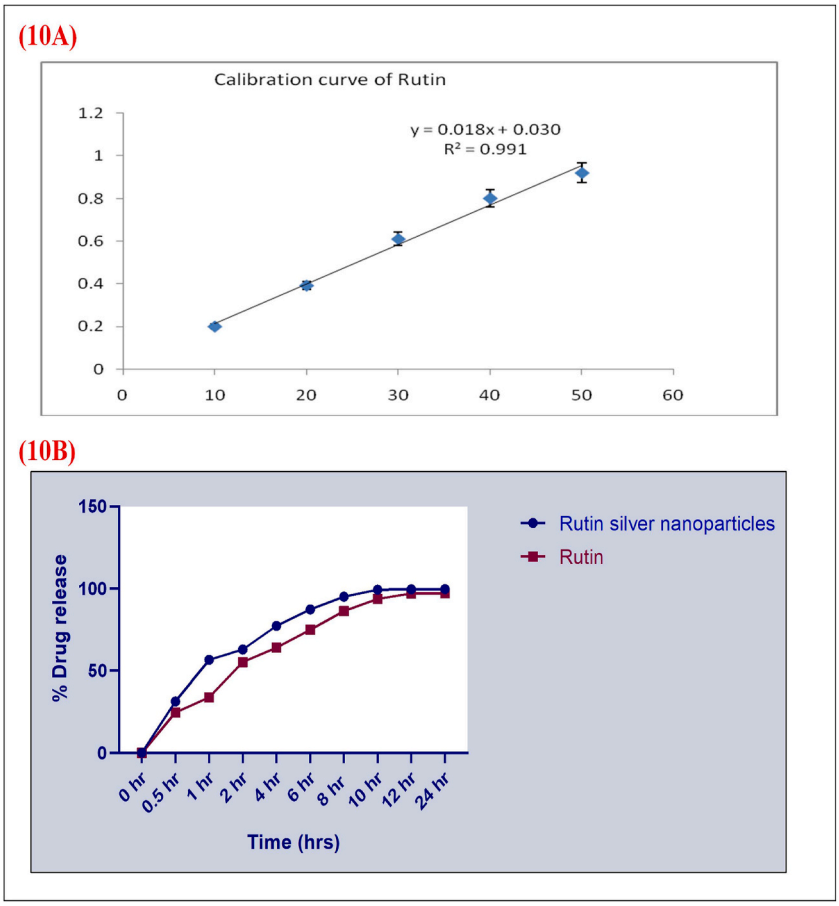

Fig. 10. (10A) Standard calibration of Rutin at 352 nm y UV–Vis Spectrophotometer, (10B) Cumulative drug release of Rutin and Rutin silver nanoparticles (F12).

9.2. *SEM and XRD for solid state stability*

The SEM studies revealed that the particles were spherical in shape with average particles in the size range of 125 nm as seen in Fig. 4A.The XRD (Shimadzu) spectrum recorded was to confirm structure cyrstallinity. The bands of diffraction were seen at 2θ values of 17.74, 21.72, 22.69, 25.24, 25.92, 28.58, 37.82, 43.43 corresponds to 110, 200, 111, 201, 002, 102, 220, and 310 respectively (JCPDS 9–432). The above observations in Fig. 4B confirm that the Rutin silver nanoparticles have hexagonal cubic lattice and crystalline nature.

9.3. *In vitro drug release studies*

The maximum wavelength of Rutin was observed at 352 nm in Fig. 10A. A graph of absorbance vs. concentration was plotted and R2 was found to be 0.991. The *In vitro* drug release studies of Rutin silver nanoparticles and the Rutin was done using USP I basket type method as in Fig. 10B. The Drug release of the Rutin silver nanoparticles was found to be 97.2 ± 0.2 at 24 h which follows super II transport according korsmeyer –peppas owed to R^2 which is > 0.89. The drug follows first order kinetics(Fig. 11A and B) with sustained release that has low dosage and reduce the side effects. The conventional Rutin has 99 % drug release in 10 h hence it has to be taken two to three times to meet maximum plasma concentrations gives in side effects on long term use. Hence Rutin silver nanoparticles are effective as Sustained release formulation which could probably decrease the dosage interval and enhance drug available for absorption at the binding. The smaller the size the greater is the drug release which was effectively proved by the *in vitro* drug release studies. The release follows first order release does not depend on the concentration. The R^2 value of the higuchi model was observed between 0.9402 and 0.977 indicates the diffusion mechanism. Peppas release exponent clearly indicates the drug release follows non-fickian diffusion mechanism at higher silver ion concentration. The effectiveness of formulating into silver nanoparticles has greater advantage for drug delivery.

9.4. Invitro antioxidant activity of optimized rutin silver nanoparticles (F12)

DPPH free radical scavenging assay: DPPH is a relatively stable free radical and the assay determines the ability of Rutin silver nanoparticles to reduce DPPH radical to the corresponding hydrazine by converting the unpaired electrons to pair once. IC_{50} values of ascorbic acid, Rutin silver nanoparticles and Rutin was found to be 30.6 ± 0.02, 49.7 ± 0.013 and 56.1 ± 0.015 μg/ml respectively as shown in Fig. 5A and B. Percentage scavenging of DPPH radical examined at different concentrations of extract, illustrates the Effect of Rutin silver nanoparticles on DPPH radicals compared to standard (Fig. 5A).

Reducing power assay: The percentage inhibition was found to be high in Rutin silver nanoparticles when compared to the Rutin alone but less than the standard. Rutin silver nanoparticles were found to have high antioxidant capacity than the Rutin and values were near to the standard which proves high antioxidant activity of Rutin silver nanoparticles (Fig. 5C).

Stability studies: The parameters such as particle size and drug release remain unchanged which ensure the characteristics of the nanoformulation. There was no significant difference observed in the samples with stability under specified conditions during the shelf life.

9.5. Invitro anticancer activity on MCF7 and G361 cell line

The anti-proliferative potential of the F12 optimized formulation was tested via MTT assay on MCF7 and G361 cell line against the standard Doxorubicin (Fig. 6A and B). The IC50values were determined and tabulated in Table 10. The histogram for cell survivability was constructed by using GraphPad Prism Software 5.0. The IC_{50} values of Rutin silver nanoparticles were found to be near to the standard thus proving its Cytotoxicity potential as anti cancer agent ($P \leq 0.005$).

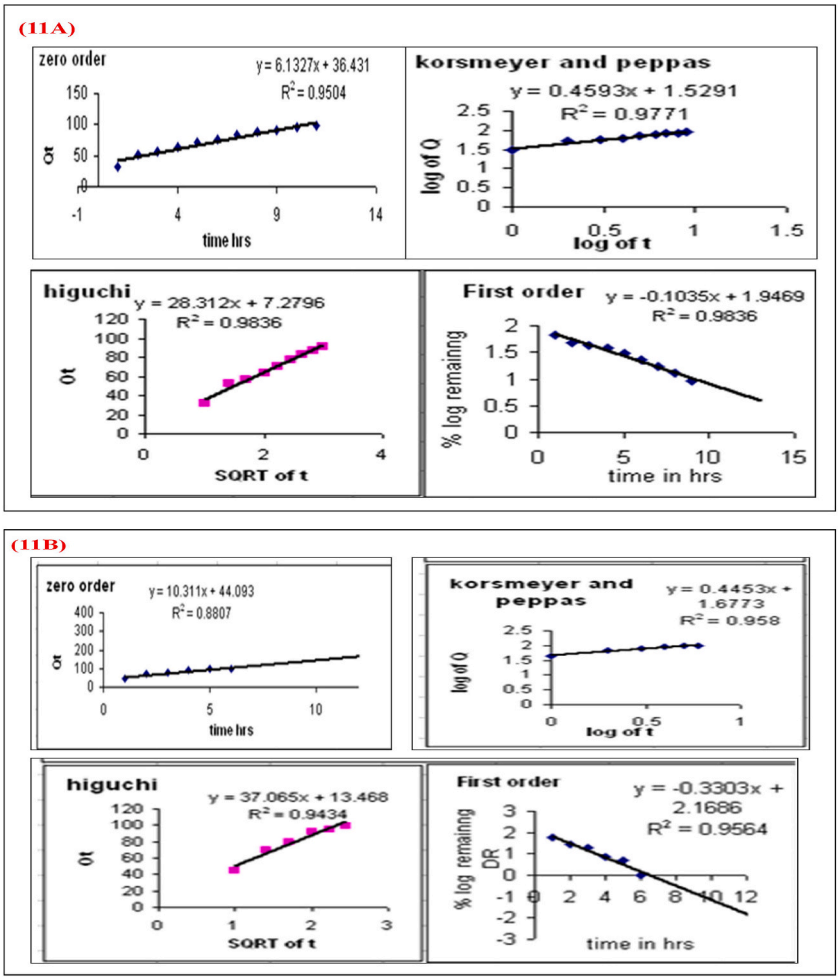

Fig. 11. (11A) Drug release kinetics of Rutin, (11B) Drug release kinetics of Rutin silver nanoparticles.

9.6. Acute oral toxicity study and effect of F12 on cyclophosphamide induced MN in bone marrow (BM) cells of mice

The test compounds did not result in any deaths at the administered dose level of 1000 mg/kg body weight for the entire 14-day observation period. Comparing the positive control cyclophosphamide with control, the positive control showed marked increase both the proportion in PCE of MN the overall MN quantity in bone marrow cells of mice (Fig. 11A). Additionally, a normal PCE/NCE ratio decline was observed. Furthermore, none of the tested doses of F12 significantly increased MN in comparison to the positive control. In the treatment groups of combined induction, F12 reduced significantly the MN frequency (CP-induced) at 0.1 and 0.2 g/kg tested dosages. Supplemental F12 addition to the usual range enhanced the PCE/NCE ratio. A dose-dependent percentage rise in MN was seen together with the positive agent cyclophosphamide. Two doses of F12 proved beneficial as a protective agent against CP. The 0.1 g/kg/bw (low dose) indicated to be more efficient 0.2 g/kg/bw dose. Table 12 and Fig. 12 A and 12B present the findings [37]. Comprehensive investigations into genotoxicity have revealed that most flavanoids, including Rutin and Rutin silver nanoparticles, yield negative results in these investigations [38–40]. The results indicated that Rutin and Rutin silver nanoparticles led to a decrease in genotoxicity by reducing the formation of reactive oxygen species (ROS).

10. Discussion

Most of the anticancer drugs lack effectiveness due to low pharmacokinetic profile, no specificity to target tumor and toxicity [6]. Thus the need of modification into nanoparticles was emphasized by most of the researchers capacitating the targeted drug delivery [2–4]. The silver nanoparticles are reported to have broad spectrum activity synthesized by green method has efficient formulation characteristics and potent bioactivity [7–10]. Thus the modified physicochemical and biological properties via conversion of herbal biomarker such as Rutin(potent anticancer agent) into silver nanoparticles is an attractive proposition and delivers a formulation with modulated particle size and less toxicity. Most of the studies on the Rutin biomarker have proven its protective and scavenging effects from free radicals [25]. Rutin administration to Sprague Drawly rats improved the CP- induced hepatotoxicity by decreasing the effect of inflammatory mediators like TNF-α, p38, IL-6, NF-κB, MAPK and COX-2 [26]. Studies suggested the attenuation of inflammation and oxidative stress induced by CP by suppression of p53 MAPK pathway. Rutin derived silver nanoparticles have been utilized as probes to detect iron ions in aqueous solution [42] and PEG loaded Rutin nanoparticles were optimized based on particle size, encapsulation efficacy and reaction time [43]. Literature supports no reports on the application of QbD approach for synthesis and optimization of Rutin silver nanoparticles. F1-F15 formulations were synthesized and optimized using QbD approach which has analyzed F12 formulation as optimized with 126 nm particles size, stable with 30 mV zeta potential, 98.2 % drug release. Production of ROS by oxidative stress induced mechanisms plays a critical role in development of lung, prostate, ovarian, liver and lung cancers. The targeted

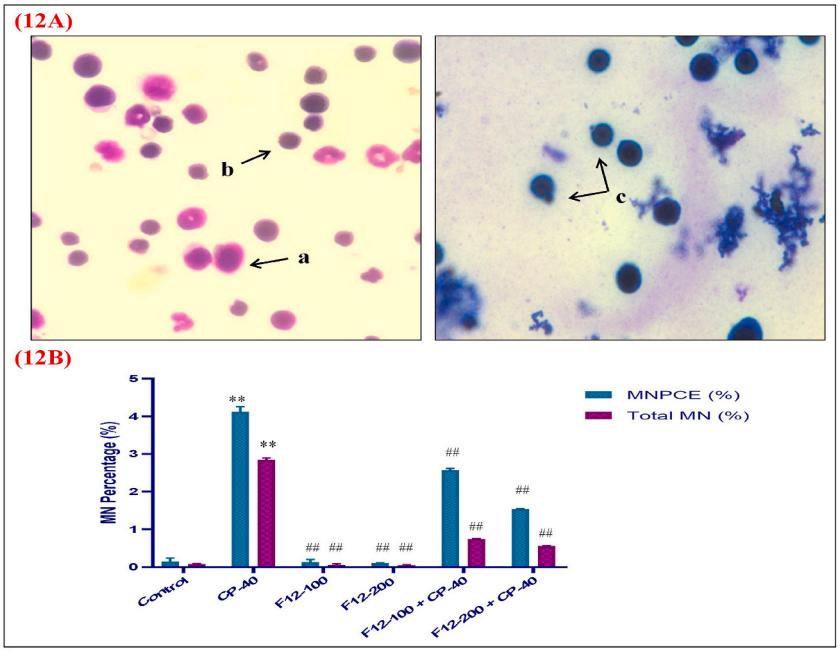

Fig. 12. Microscopic evidence of micronucleus formation in mouse bone marrow cells after cyclophosphamide treatment. (12A) a - Normochromatic erythrocytes; b - Polychromatic erythrocytes; c - Polychromatic erythrocytes with the micronucleus, (12B) Frequency of MN in Cyclophosphamide- and F12-treated mice's bone marrow cells, percentage of MNPCE (Micronucleus in polychromatic erythrocytes) and Total MN (Micronucleus in polychromatic erythrocytes and normochromatic erythrocytes) was evaluated in each mouse. Mean ± Standard Error Mean ($n = 6$), Analysis of variance (ANOVA) with a post hoc Dunnett's test. Significant at the $^{**}P < 0.001$ level when compared to the control group, $^{\#\#}P < 0.001$ when compared to cyclophosphamide. Significant decrease in number of micronuclei in the treatment group was observed.

therapy with therapeutic approach is critical interest serving the cancer biologist community [44].This formulation F12 has been studies for antioxidant activity by DPPH and H_2O_2 free radical scavenging activity as most of the cancers are induced by peroxide and superoxide free radicals. Thus the green synthesis of Rutin silver nanoparticles has proven antioxidant activity. Further the MTT assay on G361(skin cancer) and MCF7(breast cancer) cell lines was studied for morphology and IC_{50} values which has proven the cytotoxic potential. The acute toxicity studies have proven the safety dose without behavior and psychological changes till 500 mg/kg dose. The Micronucleus frequency has been significantly reduced by F12 formulation. Rutin silver nanoparticles were optimized based on QbD approach and proven with therapeutic application as antioxidants and anticancer agents. The future studies can be oriented to prove the *invivo* anticancer activity in cancer models and evaluate the underlying mechanisms.

11. Conclusion

Green synthesis is an effective, ecofriendly method that produces stable, diverse compounds of unique physicochemical properties that enhances the solubility, absorption and bioavailability of the drug. The isolation of Rutin-3-O- glycoside from the methanolic extract of the plant *Carica papaya* was reported for the first time. The characterization of Rutin-3-O- glycoside was performed using UV, HPLC, H^1 C^{13} and FTIR. The Rutin silver nanoparticles were synthesized in which the Rutin was proven to be the reducing and capping agent for silver ion. The Rutin silver nanoparticles were synthesized which could prove they were stable with 126 nm in size, −28.6 mV zeta potential without agglomeration and crystalline in nature using UV–Vis, DLS, FTIR, SEM and XRD studies. The Rutin silver nanoparticles were screened for *in vitro* antioxidant activity using DPPH free radical assay and reducing power assay which could prove that the Rutin silver nanoparticles possess the activity near to the standard and higher than the Rutin alone. Further the Rutin silver nanoparticles were screened for *in vitro* anticancer activity against the G361 and MCF cell lines against the standard doxorubicin which could prove the cytotoxic potential at 250 μg/ml. The *in vitro* drug release studies performed using the USP Dissolution apparatus I basket type could prove that the sustained release nature of the Rutin silver nanoparticles and immediate release nature of the Rutin as the Rutin silver nanoparticles follow super case II transport with first order kinetics. Thus the formulation into Rutin silver nanoparticles could enhance the antioxidant and anticancer activity and also increase the solubility of drug in water. The Rutin silver nanoparticles were found to be effective as therapeutic agents due to their nanosize and modified physicochemical properties. The Rutin silver nanoparticles could be further tested *in vivo* to establish the *in vivo-in vitro* correlation of activity and also to understand bioequivalence along with the dosage interval.

Ethical statement

The study has been conducted as per Organization of Economic cooperation and development (OECD) guideline 423 for acute toxicity studies and OECD test 473 for Bone marrow micronucleus test as per the approval obtained from the Institutional Animal Ethics Committee (IAEC) of St. Pauls College of Pharmacy in Turkayamjal, Telangana, India, thoroughly examined and granted approval for all experimental procedures (IAEC/SPCP/PCOG01/2022).

Funding

Not applicable.

Data and code availability

No data was used for the research described in the article.

CRediT authorship contribution statement

Harika Yadha: Methodology, Investigation, Formal analysis, Data curation, Conceptualization. **Rajini Kolure:** Methodology, Investigation, Formal analysis, Data curation, Conceptualization. **Sneha Thakur:** Validation, Supervision, Methodology, Investigation, Formal analysis, Data curation, Conceptualization. **Kiranmai Mandava:** Writing – review & editing, Validation, Formal analysis. **Suhasini Boddu:** Writing – review & editing, Visualization, Software, Resources.

Declaration of competing interest

The authors declare no conflicts of interest.

List of Abbreviations

UV–Vis UV–Vis spectroscopy
SEM Scanning Electron microscopy
MCF7 -Breast cancer cell line
G361 - Human skin melanoma cell line
XRD - X-ray diffraction

DLS - Dynamic light scattering

References

[1] T. Ramasamy, H.B. Ruttala, B.G. Kanu, et al., Smart chemistry-based nanosized drug delivery systems for systemic applications: a comprehensive review, J Control Rel (2017 May 1), https://doi.org/10.1016/j.jconrel.2017.04.043. Epub.

[2] I.A.M. Ali, A.B. Ahmed, H.I. Al-Ahmed, Green synthesis and characterization of silver nanoparticles for reducing the damage to sperm parameters in diabetic compared to metformin, Sci. Rep. 13 (2023) 2256, https://doi.org/10.1038/s41598-023-29412-3.

[3] T. Balamanikandan, S. Balaji, J. Pandirajan, Biological Synthesis of silver nanoparticles by using onion (Allium cepa) extract and their antibacterial and antifungal activity, World App Sci J 33 (6) (2015) 939–943, https://doi.org/10.5829/idosi.wasj.2015.33.06.9525.

[4] A. Yilmaz, M. Yilmaz, Bimetallic core-shell nanoparticles of gold and silver via bioinspired polydopamine layer as surface-enhanced Raman spectroscopy (SERS) platform, Nanomaterials 10 (2020) 688, https://doi.org/10.3390/nano10040688.

[5] Shakeel Ahmed, Mudasir Ahmad, Babu Lal Swami, Saiqa Ikram, Green synthesis of silver nanoparticles using Azadirachta indica aqueous leaf extract, Journal of radiation research and applied sciences 9 (1) (2016) 1–7, https://doi.org/10.1016/j.jrras.2015.06.006.

[6] B. Ajitha, Y. Ashok Kumar Reddy, P. Sreedhara Reddy, Biogenic nano-scale silver particles by Tephrosia purpurea leaf extract and their inborn antimicrobial activity, Spectrochim. Acta Mol. Biomol. Spectrosc. 121 (2014) 164–172, https://doi.org/10.1016/j.saa.2013.10.077.

[7] O. Abdifetah, K. Na-Bangchang, Pharmacokinetic studies of nanoparticles as a delivery system for conventional drugs and herb-derived compounds for cancer therapy: a systematic review, Int. J. Nanomed. 14 (2019) 5659–5677, https://doi.org/10.2147/IJN.S213229.

[8] R. Arshad, L. Gulshad, I. Haq, M.A. Farooq, A. Al-Farga, R. Siddique, E. Karrar, Nanotechnology: a novel tool to enhance the bioavailability of micronutrients, Food Sci. Nutr. 9 (6) (2021) 3354–3361, https://doi.org/10.1002/fsn3.2311.

[9] L. Sun, H. Liu, Y. Ye, et al., Smart nanoparticles for cancer therapy, Sig Transduct Target Ther 8 (2023) 418, https://doi.org/10.1038/s41392-023-01642-x.

[10] Swati Kumari, Sakshi Raturi, Saurabh Kulshrestha, Kartik Chauhan, Sunil Dhingra, Kovács András, Kyaw Thu, Rohit Khargotra, Tej Singh, A comprehensive review on various techniques used for synthesizing nanoparticles, J. Mater. Res. Technol. 27 (2023), https://doi.org/10.1016/j.jmrt.2023.09.291. Pg 1739-63, ISSN 2238-7854.

[11] J.A. Van den Brand, P.R. van Dijk, J.M. Hofstra, J.F. Wetzels, Cancer risk after cyclophosphamide treatment in idiopathic membranous nephropathy, Clin. J. Am. Soc. Nephrol. 9 (6) (2014 Jun 1), https://doi.org/10.2215/CJN.08880813.

[12] A. Bhattacharjee, A. Basu, P. Ghosh, J. Biswas, S. Bhattacharya, Protective effect of Selenium nanoparticle against cyclophosphamide induced hepatotoxicity and genotoxicity in Swiss albino mice, J. Biomater. Appl. 29 (2) (2014 Aug) 303–317, https://doi.org/10.1177/0885328214523323.

[13] J.A. Heddle, M.C. Cimino, M. Hayashi, F. Romagna, M.D. Shelby, J.D. Tucker, et al., Micronuclei as an index of cytogenetic damage: past, present, and future, Environ. Mol. Mutagen. 18 (4) (1991) 277–291, https://doi.org/10.1002/em.2850180414.

[14] S. Shruthi, K.B. Shenoy, Gallic acid: a promising genoprotective and hepatoprotective bioactive compound against cyclophosphamide induced toxicity in mice, Environ. Toxicol. 36 (1) (2021 Jan) 123–131, https://doi.org/10.1002/tox.23018.

[15] W. Schmid, Chemical mutagen testing on in vivo somatic mammalian cells, Agents and actions 3 (1973 Jun) 77–85, https://doi.org/10.1007/BF01986538.

[16] H.R.F. Masoumi, M. Basri, W.S. Samiun, Z. Izadiyan, C.J. Lim, Enhancement of encapsulation efficiency of nanoemulsion-containing aripiprazole for the treatment of schizophrenia using mixture experimental design, Int J Nanomedicine 10 (2015) 6469–6471, https://doi.org/10.2147/IJN.S89364.

[17] L.R. Tefas, I. Tomuță, M. Achim, L. Vlase, Development and optimization of quercetin-loaded plga nanoparticles by experimental design, Clujul Med. 88 (2) (2015) 214–223, https://doi.org/10.15386/cjmed-418.

[18] K. Narayanan, V.M. Subrahmanyam, J. Venkata Rao, A fractional factorial design to study the effect of process variables on the preparation of hyaluronidase loaded PLGA nanoparticles, Enzyme Res 2014 (2014) 162962, https://doi.org/10.1155/2014/162962.

[19] A.N. Hamed, M.E. Abouelela, A.E. El Zowalaty, M.M. Badr, M.S. Abdelkader, Chemical constituents from *Carica papaya* Linn. leaves as potential cytotoxic, EGFR wt and aromatase (CYP19A) inhibitors; a study supported by molecular docking, RSC advances 12 (15) (2022) 9154–9162, https://doi.org/10.1039/D1RA07000B.

[20] S.K. Chew, W.H. Teoh, S.L. Hong, R. Yusoff, Rutin extraction from female *Carica papaya* Linn. using ultrasound and microwave-assisted extractive methods: optimization and extraction efficiencies, Heliyon 9 (10) (2023 Oct 1) e20260, https://doi.org/10.1016/j.heliyon.2023.e20260.

[21] S.K. Chew, W.H. Teoh, S.L. Hong, R. Yusoff, Rutin extraction from female C*arica papaya* Linn. using ultrasound and microwave-assisted extractive methods: optimization and extraction efficiencies, Heliyon 9 (10) (2023 Sep 28) e20260, https://doi.org/10.1016/j.heliyon.2023.e20260. PMID: 37810831; PMCID: PMC10551569.

[22] B.K. Khor, N.J. Chear, J. Azizi, K.Y. Khaw, Chemical composition, antioxidant and cytoprotective potentials of *Carica papaya* leaf extracts: a comparison of supercritical fluid and conventional extraction methods, Molecules 26 (5) (2021 Mar 9) 1489, https://doi.org/10.3390/molecules26051489.

[23] N.A. Al-Dhabi, M.V. Arasu, C.H. Park, S.U. Park, An up-to-date review of rutin and its biological and pharmacological activities, EXCLI J 14 (2015 Jan 9) 59–63, https://doi.org/10.17179/excli2014-663. PMID: 26535031; PMCID: PMC4614038.

[24] R. Negahdari, S. Bohlouli, S. Sharifi, S. Maleki Dizaj, Y. Rahbar Saadat, K. Khezri, S. Jafari, E. Ahmadian, N. Gorbani Jahandizi, S. Raeesi, Therapeutic benefits of Rutin and its nanoformulations, Phytother Res.: PTR 35 (4) (2021) 1719–1738, https://doi.org/10.1002/ptr.6904.

[25] L.S. Chua, A review on plant-based rutin extraction methods and its pharmacological activities, J. Ethnopharmacol. 150 (3) (2013 Dec 12) 805–817, https://doi.org/10.1016/j.jep.2013.10.036. Epub 2013 Oct 30. PMID: 24184193.

[26] S. Rahmani, K. Naraki, A. Roohbakhsh, A.W. Hayes, G. Karimi, The protective effects of rutin on the liver, kidneys, and heart by counteracting organ toxicity caused by synthetic and natural compounds, Food Sci. Nutr. 11 (1) (2022 Sep 15) 39–56, https://doi.org/10.1002/fsn3.3041. PMID: 36655104; PMCID: PMC9834893.

[27] K.Y. Khaw, N.J. Chear, S. Maran, K.Y. Yeong, Y.S. Ong, B.H. Goh, Butyrylcholinesterase inhibitory activity and GC-MS analysis of *Carica papaya* leaves, Nat. Prod. Sci. 26 (2) (2020) 165–170, https://doi.org/10.20307/nps.2020.26.2.165.

[28] M. Rahimi-Nasrabadi, S.M. Pourmortazavi, S.A.S. Shandiz, F. Ahmadi, H. Batooli, Green synthesis of silver nanoparticles using *Eucalyptus leucoxylon* leaves extract and evaluating the antioxidant activities of the extract, Nat. Prod. Res. 28 (2014) 1964–1969, https://doi.org/10.1080/14786419.2014.918124.

[29] B. Ramesh, R. Rajeshwari, Anticancer activity of green synthesized silver nanoparticels of *Abutilon indicum linn*.leaf extract, Asian J. Phytomed. Clin. Res. 3 (4) (2015) 124–131.

[30] C. Krishnaraj, P. Muthukumaran, R. Ramachandran, M.D. Balakumaran, P.T. Kalaichelvan, Acalypha indica Linn: biogenic synthesis of silver and gold nanoparticles and their cytotoxic effects against MDA-MB-231, human breast cancer cells, Biotechnology Reports 4 (2014 Dec 1) 42–49, https://doi.org/10.1016/j.btre.2014.08.002.

[31] M. Kello, P. Takac, P. Kubatka, T. Kuruc, K. Petrova, J. Mojzis, Oxidative stress-induced DNA damage and apoptosis in clove buds-treated MCF-7 cells, Biomolecules 10 (1) (2020 Jan 14) 139, https://doi.org/10.3390/biom10010139.

[32] Sara A. Abouelmagd, Bo Sun, Alice C. Chang, Youn Jin Ku, Yoon Yeo, Release kinetics study of poorly water-soluble drugs from nanoparticles: are we doing it right? Mol. Pharm. 12 (3) (2015) 997–1003, https://doi.org/10.1021/mp500817h.

[33] Radhakant Gouda, Himankar Baishya, Zhao Qing, Application of mathematical models in drug release kinetics of carbidopa and levodopa ER tablets, Journal of Developing Drugs 6 (issue 2) (2017), https://doi.org/10.4172/2329-6631.1000171, 171, pg 1-8.

[34] S. Modi, B.D. Anderson, Determination of drug release kinetics from nanoparticles: overcoming pitfalls of the dynamic dialysis method, Mol. Pharm. 10 (8) (2013 Aug 5) 3076–3089, https://doi.org/10.1021/mp400154a.

[35] D. Paolino, A. Tudose, C. Celia, L. Di Marzio, F. Cilurzo, C. Mircioiu, Mathematical models as tools to predict the release kinetic of fluorescein from lyotropic colloidal liquid crystals, Materials 12 (5) (2019 Feb 26) 693, https://doi.org/10.3390/ma12050693.
[36] International Conference On Harmonisation Of Technical Requirements For Registration Of Pharmaceuticals For Human Use, Stability testing of new drug substances and products, in: ICH Harmonised Tripartite Guideline., Stability Testing of New Drug Substances and Products Q1A(R2), Current Step 4 Version Dated 6 February 2003, 2003.
[37] OECD, Test No. 474: mammalian erythrocyte micronucleus test. OECD Guidelines for the Testing of Chemicals, Section 4, OECD Publishing, Paris, 2016, https://doi.org/10.1787/9789264264762-en.
[38] J. Da Silva, S.M. Herrmann, V. Heuser, W. Peres, N.P. Marroni, J. González-Gallego, B. Erdtmann, Evaluation of the genotoxic effect of Rutin and quercetin by comet assay and micronucleus test, Food Chem. Toxicol. 40 (7) (2002 Jul 1) 941–947, https://doi.org/10.1016/S0278-6915(02)00015-7.
[39] J. Sanz-Serrano, A. Vettorazzi, D. Muruzabal, A.L. de Cerain, A. Azqueta, In vitro genotoxicity assessment of functional ingredients: DHA, Rutin and α-tocopherol, Food Chem. Toxicol. 153 (2021 Jul 1) 112237, https://doi.org/10.1016/j.fct.2021.112237.
[40] A. Shahid, R. Ali, N. Ali, S. Kazim Hasan, S. Rashid, F. Majed, S. Sultana, Attenuation of genotoxicity, oxidative stress, apoptosis and inflammation by Rutin in benzo (a) pyrene exposed lungs of mice: plausible role of NF-κB, TNF-α and Bcl-2, J. Compl. Integr. Med. 13 (1) (2016 Mar 1) 17–29, https://doi.org/10.1515/jcim-2015-0078.
[41] OECD guideline, Acute toxic class method, Test No. 423: Acute Oral toxicity - Acute Toxic Class Method. OECD Guidelines for the Testing of Chemicals, Section 4 : Health Effects | OECD iLibrary n.d. https://doi.org/10.1787/9789264071001-en.
[42] M.S. Coutinho, E. Latocheski, J.M. Neri, A.C.O. Neves, J.B. Domingos, L.N. Cavalcanti, F.G. Menezes, Rutin-modified silver nanoparticles as a chromogenic probe for the selective detection of Fe3+ in aqueous medium, RSC Adv. 9 (51) (2019) 30007–30011, https://doi.org/10.1039/c9ra06653e.
[43] K. Kızılbey, Optimization of rutin-loaded PLGA nanoparticles synthesized by single-emulsion solvent evaporation method, ACS Omega 4 (1) (2019) 555–562, https://doi.org/10.1021/acsomega.8b02767.
[44] M.J. Iqbal, A. Kabeer, Z. Abbas, et al., Interplay of oxidative stress, cellular communication and signaling pathways in cancer, Cell Commun. Signal. 22 (2024) 7, https://doi.org/10.1186/s12964-023-01398-5.